Nano Research 2015, 8(4): 1348–1356
DOI 10.1007/s12274-014-0626-5
Research Article
ISSN 1998-0124
CN 11-5974/O4

A density functional theory study of the tunable structure, magnetism and metal–insulator phase transition in VS_2 monolayers induced by in-plane biaxial strain

Min Kan[1,2,3], Bo Wang[4], Young Hee Lee[2,3] (✉), and Qiang Sun[1,5] (✉)

[1] *Department of Materials Science and Engineering, Peking University, Beijing 100871, China*
[2] *Center for Integrated Nanostructure Physics, Institute for Basic Science, Sungkyunkwan University, Suwon 440-746, Korea*
[3] *Department of Physics and Department of Energy Science, Sungkyunkwan University, Suwon 440-746, Korea*
[4] *School of Mathematical Sciences, Peking University, Beijing 100871, China*
[5] *Center for Applied Physics and Technology, Peking University, Beijing 100871, China*

Received: 18 August 2014
Revised: 7 October 2014
Accepted: 28 October 2014

© Tsinghua University Press and Springer-Verlag Berlin Heidelberg 2014

KEYWORDS
phase transition,
biaxial strain,
phase diagram,
density functional theory (DFT),
transition metal dichalcogenide (TMD) materials

ABSTRACT

We report a density functional theory study of a phase transition of a VS_2 monolayer that can be tuned by the in-plane biaxial strain. This results in both a metal–insulator transition and a low spin–high spin magnetic transition. At low temperature, the semiconducting H-phase is stable and large strain (>3%) is required to provoke the transition. On the other hand, at room temperature (300 K), only a small tensile strain of 2% is needed to induce the phase transition from the semiconducting H-phase to the metallic T-phase together with the magnetic transition from high spin to low spin. The phase diagram dependence on both strain and temperature is also discussed in order to provide a better understanding of the phase stability of VS_2 monolayers.

1 Introduction

Two-dimensional (2D) layered transition metal dichalcogenide (TMD) materials have been intensively studied recently because of their unique properties that give rise to potential uses in catalysis, energy storage, integrated circuits, transparent conducting electrodes, optoelectronics, and valleytronics [1–5]. TMDs materials have the chemical formula MX_2, where M is a transition metal and X is a chalcogen (X = S, Se, Te). Depending on the combination of chalcogen and transition metal, more than 40 different TMDs

Address correspondence to Young Hee Lee, leeyoung@skku.edu; Qiang Sun, sunqiang@pku.edu.cn

can be realized, which can be metallic, semimetallic, or semiconducting [6, 7]. Different experimental strategies have been used to synthesize TMD monolayers successfully, such as mechanical exfoliation methods, liquid exfoliation methods, and chemical vapor deposition (CVD) [8–10], which have stimulated the search for unprecedented physical and chemical properties from a theoretical point of view.

Monolayer TMD materials can in general exhibit two polymorphs: Trigonal prismatic (denoted the H-phase) and octahedral coordinated (denoted T-phase) [11]. The H-phase has the space group $P\bar{6}m2$ and belongs to the D_{3h} point group, while the T-phase belongs to the D_{3d} point group. It is intriguing to see that the electronic and magnetic properties of the two such polymorphs are quite different from each other. For example, the H-phase MoS_2 monolayer is a direct semiconductor with a band gap around 1.90 eV [12], while the T-phase MoS_2 monolayer is metallic. Thus, it will be fascinating if one can reversibly control the phase transition between H-phase and T-phase TMDs, since this will have great potential applications in future electronic devices.

Recently, significant progress has been achieved in the synthesis of WS_2 nanotubes with octahedral coordination using rhenium doping [13], which is an irreversible process. More interestingly, it has been recently shown that the T-phase MoS_2 monolayer can coexist in a layer of the Re-doped H-phase MoS_2 under electron beam irradiation at high temperature [14]. In this case, chemical doping, electronic beam, and temperature effects are combined to give partial conversion to the T-phase, which is hard to realize reversibly in devices. It has been also proposed theoretically that electron injection with a concentration of 8.33×10^{14} cm^{-2} or lithium adsorption with a concentration of exactly 20% can also induce the phase transition for MoS_2 monolayers from the H-phase to the T-phase [15]; however, this electron concentration is quite high and the extent of lithium adsorption on the surface is uncontrollable in experiments. Very recently, ultrathin 2D VS_2 nanosheets have been successfully synthesized by a hydrothermal method [16, 17], and demonstrated room temperature ferromagnetism and hysteresis in a 2D structure for the first time [17]. A question then arises: Can we find a controllable, reversible and experimentally feasible method to induce the phase transition between H and T phases in TMD materials in order to change the electronic and magnetic properties?

In this study, we show that the electronic and magnetic properties of monolayer T-phase and H-phase VS_2 are quite different from each other. The T-phase VS_2 is metallic, while the H-phase VS_2 is a semiconductor with a band gap of 0.187 eV. The magnetic moment of the T-phase per unit cell is 0.43 μ_B, while that of the H-phase VS_2 is an integer of 1.0 μ_B. By simply applying a biaxial compression or tensile strain, we can reversibly tune the phase stability of VS_2. Previously, in-plane strain has been extensively used to tune the electronic and magnetic properties of 2D materials. For example, the magnetic moments of MX_2 (M = V, Nb; X = S, Se) can be enhanced significantly by tensile strain [18, 19]. As far as we know, this is the first study using the in-plane strain to tune the phase stability of 2D TMD materials. For a VS_2 sheet at 0 K, the H-phase is stable in the biaxial strain range $-7\% < \varepsilon < 4.5\%$, while the T-phase is more stable than the H-phase when $\varepsilon < -7\%$ and $\varepsilon > 4.5\%$. By considering the temperature effect, a tensile strain less than 2%, which is accessible in experiments, can reverse the phase stability from the H-phase to the T-phase at room temperature (300 K). We also simulate the phase diagram of monolayer VS_2 by including the strain and temperature effects together, which helps to better understand the phase transition of monolayer VS_2.

2 Computational methods

Our first-principles calculations are based on spin-polarized density functional theory (DFT) with the Perdew–Burke–Ernzerhof (PBE) form and the generalized gradient approximation (GGA) [20] for exchange-correlation potential. Plane-wave basis sets with the projector augmented plane-wave method (PAW) [21] are used as implemented in the Vienna *ab initio* simulation package (VASP) [22]. Periodic boundary conditions are used to simulate 2D monolayer VS_2 and all the structures are relaxed without any symmetry constraints. A vacuum space of 30 Å is used along the *c*-axis in order to avoid interactions between two neighboring images. The reciprocal

space is represented by a Monkhorst–Pack special k-point scheme [23] with 25 × 25 × 1 and 9 × 9 × 1 grid meshes for a unit cell and a (4 × 4) supercell. For geometry optimization, the criteria of convergence for energy and force, as well as energy cutoff are set to be 1×10^{-8} eV, 1×10^{-6} eV/Å, and 400 eV, respectively. To properly describe the strongly correlated electrons in the partially filled d subshells, we use the GGA + U_{eff} method introduced by Dudarev et al. [24] with U_{eff} = 3.0 eV for V atoms, which has been widely used in previous reports [25–27]. In addition, the state-of-the-art hybrid functional (HSE06) [28, 29] is also employed to calculate the band structures. Calculations of the thermal properties are performed using finite displacement method as implemented in the Phonopy program [30] and 4 × 4 supercells containing 48 atoms are employed. The Helmholtz free energy (F) contains two contributions: Total energy E_0 at 0 K and phonon free energy F_{ph}, and can be written as $F(T) = E_0 + F_{\text{ph}}(T)$. As written in the manual of Phonopy program, the phonon free energy F_{ph} is calculated from the following equations

$$F_{\text{ph}}(T)=\frac{1}{2}\sum_{q,s}\hbar\omega(\boldsymbol{q},s)+k_{\text{B}}T\sum_{q,s}\ln[1-\exp(-\hbar\omega(\boldsymbol{q},s)/k_{\text{B}}T)]$$

where k_{B} and $\hbar$ are the Boltzmann constant and the reduced Planck's constant, respectively, and $\omega(\boldsymbol{q}, s)$ stands for the s^{th} phonon frequency with a wave vector $\boldsymbol{q}$ at 0 K. The variations in the temperature-dependent electron occupation and electron–phonon coupling are neglected.

3 Result and discussion

We first perform fully relaxed structure optimization for both the T-phase and H-phase of a VS_2 monolayer. The optimized structures and calculated geometric parameters are shown in Fig. 1 and Table 1, respectively. For the T-phase (H-phase), the lattice constant, V–S bond length, and the distance between the V and S atom planes are 3.181 (3.173), 2.351 (2.362) and 1.468 (1.491) Å, respectively, which agree very well with a previous study [31] using the same exchange-correlation potential. We also calculate the cohesive energy per unit cell, which is defined as $E_{\text{C}} = -(E_{\text{VS2}} - E_{\text{V}} - 2E_{\text{S}})$, where E_{VS2} stands for the energy of VS_2 per unit cell, and E_{V} and E_{S} are the energy of free V and S atoms, respectively. The calculated cohesive energies are 15.20 and 15.25 eV per VS_2 chemical unit for the H- and T-phase, respectively, indicating strong cohesive bonds for two phases; these values should be compared to the overestimated local-density approximation (LDA) result (17.5 eV) [32]. The calculated band structure using the PBE functional is shown in Figs. 2(a) and 2(b), indicating that the T-phase of VS_2 monolayer is metallic which is in agreement with previous theoretical and experimental studies [16, 18, 31, 32], while the H-phase is an indirect semiconductor with a small band gap of 0.187 eV.

Since GGA fails to give an accurate band gap for TMD semiconductors, we use GGA+U and state-of-the-art hybrid functional HSE06 to further confirm the semiconducting property of H-phase VS_2 monolayer in the following. Based on previous studies [25–27], we use U_{eff} = 3.0 eV to calculate the band structure, as shown in Fig. 2(c). By introducing strong correlation in d subshells of V atoms, the band gap increases to 0.721 eV. In the calculation with HSE06, we also get a semiconductor character from the band structure in

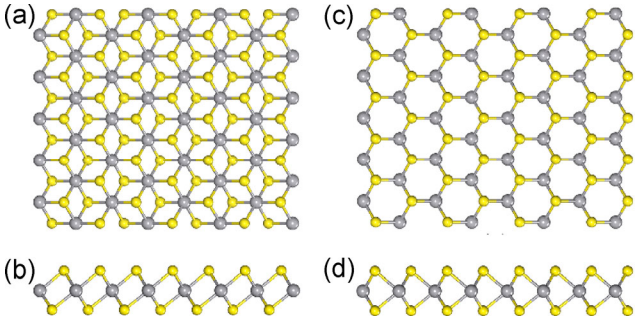

Figure 1 (a) Top view and (b) side view geometry of T-phase monolayer VS_2; (c) top view and (d) side view geometry of H-phase monolayer VS_2 where V atoms are gray and S atoms are yellow.

Table 1 The optimized geometrical parameters, cohesive energy, and band gap for T-phase and H-phase VS_2: Lattice parameter, a_0; bond length, $d_{\text{V–S}}$; interlayer distance between vanadium and sulfur planes, $\Delta_{\text{V–S}}$; V–S–V bond angle, $\theta_{\text{V–S–V}}$; cohesive energy per VS_2 unit, E_{C}; band gap calculated from PBE, E_{g}

	a_0 (Å)	$d_{\text{V–S}}$ (Å)	$\Delta_{\text{V–S}}$ (Å)	$\theta_{\text{V–S–V}}$ (°)	E_{C} (eV)	E_{g} (eV)
T	3.181	2.351	1.468	85	15.25	0
H	3.173	2.362	1.491	84	15.20	0.187

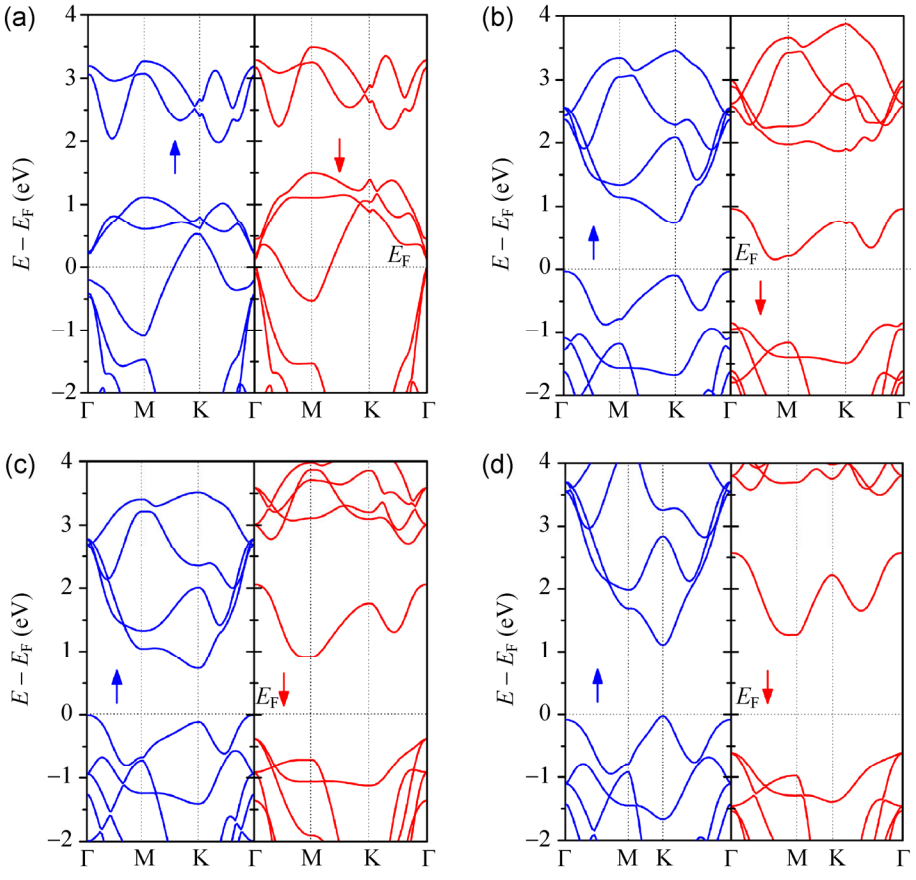

Figure 2 Calculated band structures of (a) T-phase and (b) H-phase VS_2 with the PBE method; the calculated band structure of H-phase VS_2 with (c) GGA+U (U = 3.0 eV) and (d) HSE06 method.

Fig. 2(d), and the band gap is further increased to 1.128 eV. This ensures that H-phase VS_2 monolayer is a semiconductor in spite of some numerical variance with calculation methods. To get a precise value of the band gap, one needs to use GW calculation methods [33]. However, due to limited computational resources, we still used the PBE method in the following to study the phase transition.

In addition, we also carry out spin-polarized calculations to study the magnetic properties of monolayer T-phase VS_2 and H-phase VS_2. The calculated magnetic moment of T-phase VS_2 per unit cell is 0.43 μ_B, and that of H-phase VS_2 is 1.0 μ_B, which is almost twice that for T-phase monolayer VS_2. This is consist with previous studies [17, 31] and can be understood in terms of the electronic configurations of T-phase VS_2 and H-phase VS_2: In the T-phase, both the spin-up and spin-down bands are metallic, and the $3d^1$ electron partially occupies the two polarized bands leading to a fractional magnetic moment of less than 1.0 μ_B. On the other hand, the H phase adopts a trigonal-prismatic structure, and the d orbitals of the V atom are divided into three groups, a_1' (d_{z^2}), e' (d_{xy} and $d_{x^2-y^2}$) and e'' (d_{yz} and d_{xz}) [34, 35]. Previous calculations indicate that the a_1' orbital is the lowest d level [35], and the spin-up and spin-down states are totally separated as shown in Fig. 2(b). Thus, the single $3d^1$ electron will fully occupy one of the two spin polarized d_{z^2} orbitals, resulting in a integral magnetic moment of 1.0 μ_B per unit cell and a band gap between the spin-up and spin-down a_1' orbitals. The iso-surfaces of the spin density ($\rho\uparrow - \rho\downarrow$) for T-phase VS_2 and H-phase VS_2 are shown in Fig. 3, and indicate that the V atoms in the H-phase are more spin-polarized than those in the T-phase.

Since the electronic and magnetic properties are quite different for two phases, as we discussed above, it will be quite interesting to see if we can realize the

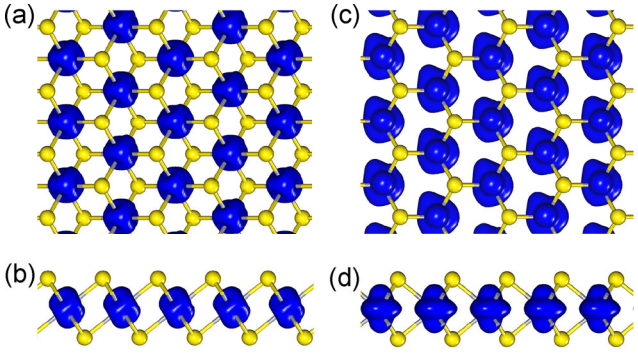

Figure 3 Iso-surface (with value of 0.05 electron/Å^3) on (a) top view and (b) side view of spin density of 2D T-phase VS_2; iso-surface (with value of 0.05 electron/Å^3) on (a) top view and (b) side view of spin density of 2D H-phase VS_2. In the iso-surface plot, blue represents positive values.

phase transition between H-phase and T-phase VS_2 in a tenable way by experiment. Additionally, a previous study shows that the energy barrier between the two phases is 0.62 eV [31], which is much smaller than that in MoS_2. These results indicate that the phase transition in VS_2 should be easier to realize. Recent studies suggest that elastic strain engineering can be used to manipulate the physical properties of low-dimensional materials, which allows a much wider dynamic range of elastic strain to be reached reversibly [18, 19, 36–38]. Thus, we propose that a biaxial tensile or compressive strain may induce the phase transition between our two phases of monolayer VS_2. Here, we define the biaxial strain as $\varepsilon = (a - a_0)/a_0 \times 100\%$, where a_0 (3.173 Å) is the lattice constant of the H-phase VS_2 in its equilibrium state, and a is the lattice constant of the strained monolayer VS_2. The smooth variations of total energies per unit cell with biaxial strain from –10% to 10% are shown in Fig. 4. The H-phase is more stable than the T-phase in the range $-7\% < \varepsilon < 4.5\%$ as marked in green, while the T-phase is more stable than the H-phase in the range $-10\% < \varepsilon < -7\%$ and $4.5\% < \varepsilon < 10\%$, as marked with yellow in Fig. 4(a). The phase transition from the H-phase to the T-phase occurs at a compressive strain of 7% and a tensile strain of 4.5%. To our knowledge, such a strain-induced phase transition between the T-phase and H-phase has never been observed in other TMD materials, which can be ascribed to the small energy difference between two phases of VS_2. We also tried to induce the phase transition for MoS_2 with the same method but failed due to the large energy difference between the two phases of MoS_2.

To check the possibility of potential applications of monolayer VS_2 in spintronic and electronic devices, we also calculated the variations in band gap and magnetic moment with different strains. Even though a low-dimensional material can in general sustain a larger strain without fracture than a bulk material, we only simulate the strain between –4% and 4% in the following, taking into account values that can be realized experimentally. The band gap of the T-phase is always 0 eV, independent of the studied strain value. On the other hand, the band gap of the H-phase varies as the strain changes. The H-phase retains semiconducting behavior without an appreciable change in band gap under tensile strain, while it converts to a metallic phase with a compressive strain of $\leqslant -3\%$. Figure 4(c) shows that the H-phase possesses an integral magnetic moment of 1 μ_B when the strain $\geqslant -2\%$, while it possesses a fractional magnetic moment with a strain $\leqslant -3\%$. The T-phase always possesses a fractional magnetic moment and the magnetic moment increases monotonically as the strain increases from –4% to 4%, which is consistent with a previous study [18]. We also find that the magnetic moment of the H-phase is always larger than that of the T-phase for each given strain, so that the H-phase can be defined as a high magnetic moment state, and the T-phase as a low magnetic moment state. Our calculations predict that both the metal–insulator transition and the high spin–low spin magnetic transition can occur simultaneously by simply tuning the biaxial strain.

The above DFT simulations of the phase transition induced by strain above were carried out at 0 K. However, in reality, the temperature is also an important factor associated with the influence of strain on phase stability. One famous example is the Peierls phase transition, which has already been found in one-, two- and three-dimensional systems [39–41]. A recent study showed that when the temperature is increased, the phase transition in MoS_2 is easier to realize [14]. Hence we also studied the phase transition of our 2D VS_2 system by considering the temperature effect. First, we simulate the Helmholtz free energy for both H-phase and T-phase VS_2 monolayers without strain

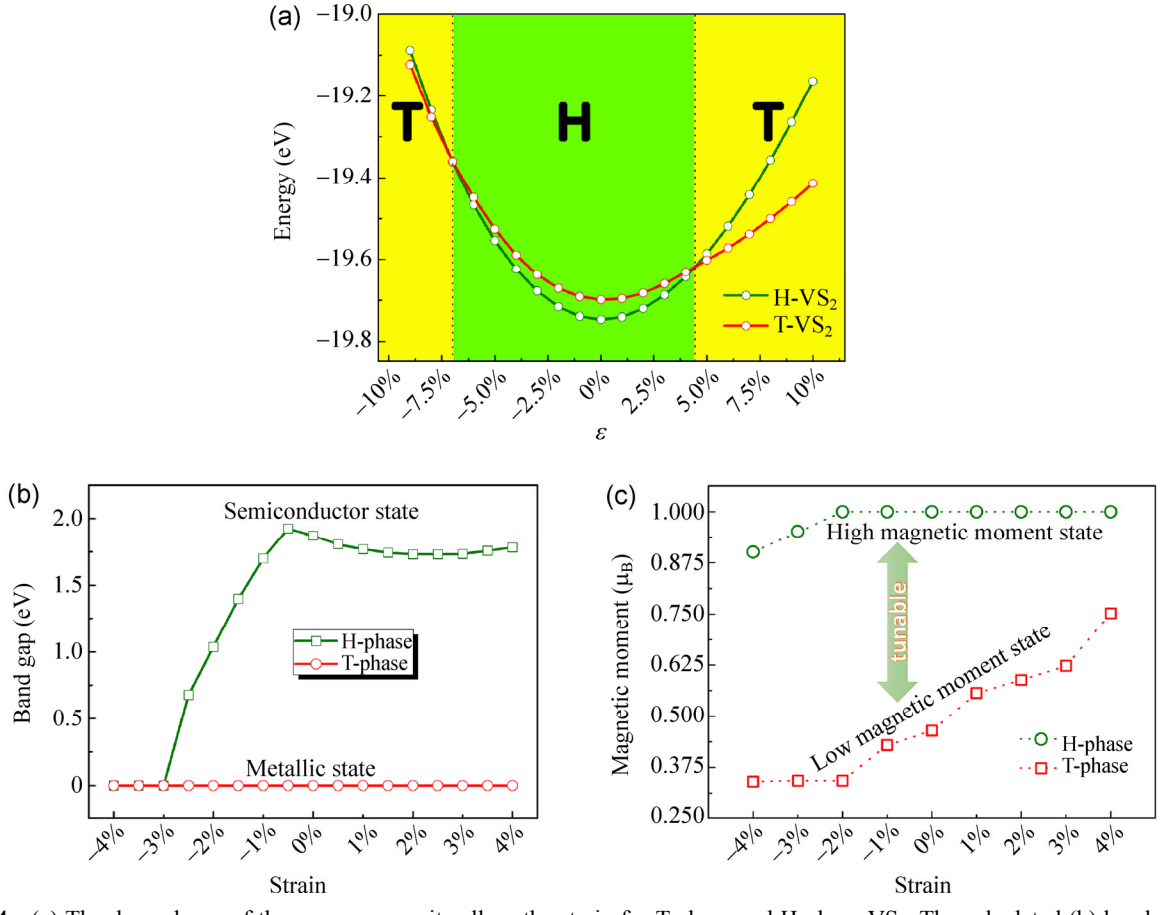

Figure 4 (a) The dependence of the energy per unit cell on the strain for T-phase and H-phase VS_2. The calculated (b) band gap and (c) the dependence of the magnetic moments for T-phase and H-phase monolayer VS_2 on the biaxial strain.

as shown in Fig. 5(a), which shows the typical free energy curves. At low temperature, the free energy of the H-phase is smaller than that of the T-phase and the difference decreases as the temperature increases. Interestingly, the stability of the two phases is reversed at a critical temperature (T_P). To check the critical temperature carefully, we also plot the Helmholtz free energy difference between H-phase and T-phase VS_2, which is defined as $\Delta F_{H-T} = F_{H\text{-phase}} - F_{T\text{-phase}}$. From Fig. 5(b), we can see that the critical point is 502 K, indicating the H-phase is more stable than the T-phase from 0 to 502 K and the T-phase is more stable than the H-phase when the temperature is higher than 502 K. Thus, the temperature effect is indeed an important factor that can influence the phase stability of our 2D monolayer VS_2.

From the above simulations, we know that at 0 K the H-phase is stable in the biaxial strain range –7% < ε < 4.5%, while the T-phase is more stable than the H-phase when ε < –7% and ε > 4.5%; without strain, the H-phase is stable from 0 to 502 K, and the T-phase is more stable than the H-phase when the temperature is higher than 502 K. The next question is whether or not the temperature effect can lower the critical strain, and what the phase diagram will look like when both strain and temperature effects are considered. In the following, we calculate the critical temperature for the 2D monolayer VS_2 at each strain and fit a phase boundary between H-phase and T-phase VS_2. The critical temperature is obtained when $F_{H\text{-phase}}(T_p) = F_{T\text{-phase}}(T_p)$.

The final simulated phase diagram, incorporating the dependence on biaxial strain and temperature, of the 2D monolayer VS_2 is shown in Fig. 5(c). As we can see from the phase diagram, there is a distinct boundary between the H-phase and T-phase, which

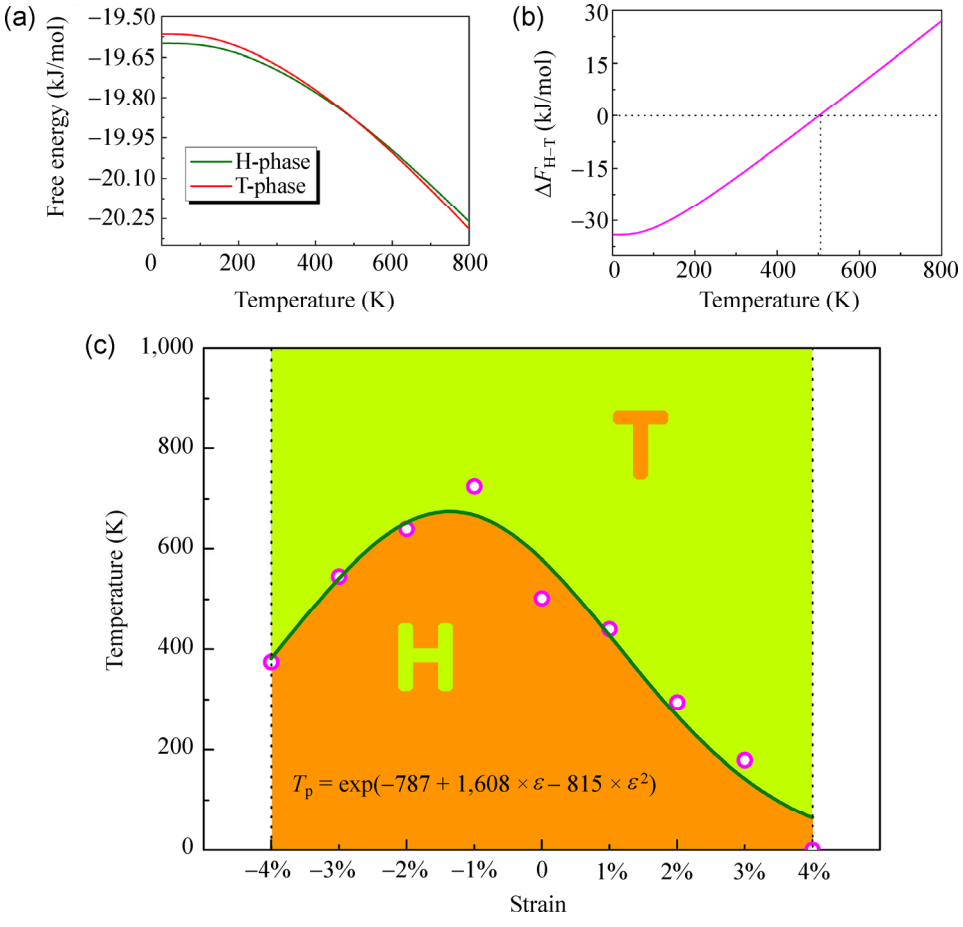

Figure 5 (a) Calculated Helmholtz free energy for H-phase and T-phase VS_2 monolayers; (b) the Helmholtz free energy difference between H-phase and T-phase VS_2; (c) simulated dependence of the phase diagram of 2D monolayer VS_2 on the biaxial strain and temperature.

is marked in green and can be fitted to the formula

$$T = \exp(-787 + 1{,}608 \times \varepsilon - 815 \times \varepsilon^2)$$

In the low temperature region (< 300 K), most of the phase diagram is filled with the H-phase, and the T-phase can only be more stable than H-phase when an appropriate biaxial tensile strain is applied. For example, a 2% biaxial tensile strain is required to reach the T-phase at 300 K. In the high temperature region (> 700 K), the T-phase is always more stable than H-phase within the biaxial strain range from –4% to 4%. At a typical temperature such as 500 K, we have the chance to realize the phase transition T→H→T as the biaxial strain increases from –4% to 4%. More importantly, at room temperature (300 K), the H-phase is more stable when the biaxial strain is smaller than 2%. This means that a biaxial tensile strain of only 2%, which is easily accessible in experiments, can tune the phase stability from H-phase to T-phase for monolayer VS_2 and vice versa. To our knowledge, this is the first example where such a small strain can induce a phase transition in 2D monolayer TMD materials. One general conclusion is that the H-phase will be more stable as the temperature decreases, while the T-phase will be more stable as the temperature increases, at each strain between –4% and 4% in our simulation. Another result associated with the mountain shape of the phase boundary is that the temperature effect can lower the critical strain in VS_2 monolayers. This synergetic effect on the phase transition may be employed experimentally in areas such as electronic memory devices or CVD growth, where strain always exists due to the lattice mismatch between the TMD material and the substrate. Thus, we hope that our simulation data can guide further experimental studies of strain sensors and low-wavelength photodetectors.

4 Conclusions

To explore the phase transition of monolayer VS_2, we performed first-principles calculations by applying biaxial compressive and tensile strain. The following conclusions can be drawn: (i) The electronic properties of T-phase and H-phase VS_2 are quite different from each other, with the former being a metal while the latter a semiconductor; (ii) both T-phase and H-phase VS_2 are magnetic, with the H-phase VS_2 possessing a magnetic moment of 1.0 μ_B which is almost twice that of the T-phase; (iii) the biaxial strain can be used to tune the phase stability. At 0 K, the H-phase is stable in the strain range $-7\% < \varepsilon < 4.5\%$, while the T-phase is more stable than the H-phase for $-10\% < \varepsilon < -7\%$ and $4.5\% < \varepsilon < 10\%$; (iv) at room temperature (300 K), a tensile strain less than 2%, which is accessible in experiments, can reverse the phase stability from the H-phase to the T-phase; (v) the strain can induce the phase transition between two phases from metal to insulator, and from low spin to high spin magnetism; (vi) the dependence of the phase diagram of monolayer VS_2 on the temperature and strain can be simulated, and the relationship between the critical temperature and critical strain can be expressed as $T_P = \exp(-787 + 1{,}608 \times \varepsilon - 815 \times \varepsilon^2)$. Compared to the existing strategies for inducing a phase transition between the T-phase and H-phase in TMD materials, our proposal of strain associated with temperature is reversible and should be feasible experimentally.

Acknowledgements

This work is partially supported by grants from the National Natural Science Foundation of China (Nos. 21173007 and 11274023), and from the National Basic Research Program of China (No. 2012CB921404), and the Institute for Basic Science in Korea.

References

[1] Ponomarenko, L. A.; Schedin, F.; Katsnelson, M. I.; Yang, R.; Hill, E. W.; Novoselov, K. S.; Geim, A. K. Chaotic dirac billiard in graphene quantum dots. *Science* **2008**, *320*, 356–358.

[2] Wang, X. R.; Li, X. L.; Zhang, L.; Yoon, Y.; Weber, P. K.; Wang, H. L.; Guo, J.; Dai, H. J. N-doping of graphene through electrothermal reactions with ammonia. *Science* **2009**, *324*, 768–771.

[3] Wang, X.; Zhi, L. J.; Müllen, K. Transparent, conductive graphene electrodes for dye-sensitized solar cells. *Nano Lett.* **2007**, *8*, 323–327.

[4] Eda, G.; Yamaguchi, H.; Voiry, D.; Fujita, T.; Chen, M. W.; Chhowalla, M. Photoluminescence from chemically exfoliated MoS_2. *Nano Lett.* **2011**, *11*, 5111–5116.

[5] Mak, K. F.; He, K. L.; Shan, J.; Heinz, T. F. Control of valley polarization in monolayer MoS_2 by optical helicity. *Nat. Nanotechnol.* **2012**, *7*, 494–498.

[6] Marseglia, E. A. Transition metal dichalcogenides and their intercalates. *Int. Rev. Phys. Chem.* **1983**, *3*, 177–216.

[7] Wilson, J. A.; Yoffe, A. D. The transition metal dichalcogenides discussion and interpretation of the observed optical, electrical and structural properties. *Adv. Phys.* **1969**, *18,* 193–335.

[8] Radisavljevic, B.; Radenovic, A.; Brivio, J.; Giacometti, V.; Kis, A. Single-layer MoS_2 transistors. *Nat. Nanotechnol.* **2011**, *6*, 147–150.

[9] Lee, C.; Li, Q. Y.; Kalb, W.; Liu, X. Z.; Berger, H.; Carpick, R. W.; Hone, J. Frictional characteristics of atomically thin sheets. *Science* **2010**, *328*, 76–80.

[10] Wang, Q. H.; Kalantar-Zadeh, K.; Kis, A.; Coleman, J. N.; Strano, M. S. Electronics and optoelectronics of two-dimensional transition metal dichalcogenides. *Nat. Nanotechnol.* **2012**, *7*, 699–712.

[11] Chhowalla, M.; Shin, H. S.; Eda, G.; Li, L. J.; Loh, K. P.; Zhang, H. The chemistry of two-dimensional layered transition metal dichalcogenide nanosheets. *Nat. Chem.* **2013**, *5*, 263–275.

[12] Mak, K. F.; Lee, C.; Hone, J.; Shan, J.; Heinz, T. F. Atomically thin MoS_2: A new direct-gap semiconductor. *Phys. Rev. Lett.* **2010**, *105*, 136805.

[13] Enyashin, A. N.; Yadgarov, L.; Houben, L.; Popov, I.; Weidenbach, M.; Tenne, R.; Bar-Sadan, M.; Seifert, G. New route for stabilization of 1T-WS_2 and MoS_2 phases. *J. Phys. Chem. C* **2011**, *115*, 24586–24591.

[14] Lin, Y. C.; Dumcenco, D. O.; Huang, Y. S.; Suenaga, K. Atomic mechanism of the semiconducting-to-metallic phase transition in single-layered MoS_2. *Nat. Nanotechnol.* **2014**, *9*, 391–396.

[15] Kan, M.; Wang, J. Y.; Li, X. W.; Zhang, S. H.; Li, Y. W.; Kawazoe, Y.; Sun, Q.; Jena, P. Structures and phase transition of a MoS_2 monolayer. *J. Phys. Chem. C* **2014**, *118*, 1515–1522.

[16] Feng, J.; Sun, X.; Wu, C. Z.; Peng, L.; Lin, C. W.; Hu, S. L.; Yang, J. L.; Xie, Y. Metallic few-layered VS_2 ultrathin

nanosheets: High two-dimensional conductivity for in-plane supercapacitors. *J. Am. Chem. Soc.* **2011**, *133*, 17832–17838.

[17] Gao, D. Q.; Xue, Q. X.; Mao, X. Z.; Wang, W. X.; Xu, Q.; Xue, D. S. Ferromagnetism in ultrathin VS_2 nanosheets. *J. Mater. Chem. C* **2013**, *1*, 5909–5916.

[18] Ma, Y. D.; Dai, Y.; Guo, M.; Niu, C. W.; Zhu, Y. T.; Huang, B. B. Evidence of the existence of magnetism in pristine VX_2 monolayers (X = S, Se) and their strain-induced tunable magnetic properties. *ACS Nano* **2012**, *6*, 1695–1701.

[19] Zhou, Y. G.; Wang, Z. G.; Yang, P.; Zu, X. T.; Yang, L.; Sun, X.; Gao, F. Tensile strain switched ferromagnetism in layered NbS_2 and $NbSe_2$. *ACS Nano* **2012**, *6*, 9727–9736.

[20] Perdew, J. P.; Burke, K.; Ernzerhof, M. Generalized gradient approximation made simple. *Phys. Rev. Lett.* **1996**, *77*, 3865–3868.

[21] Kresse, G.; Joubert, D. From ultrasoft pseudopotentials to the projector augmented-wave method. *Phys. Rev. B* **1999**, *59*, 1758–1775.

[22] Kresse, G.; Furthmüller, J. Efficient iterative schemes for *ab initio* total-energy calculations using a plane-wave basis set. *Phys. Rev. B* **1996**, *54*, 11169–11186.

[23] Monkhorst, H. J.; Pack, J. D. Special points for Brillouin-zone integrations. *Phys. Rev. B* **1976**, *13*, 5188–5192.

[24] Dudarev, S. L.; Botton, G. A.; Savrasov, S. Y.; Humphreys, C. J.; Sutton, A. P. Electron-energy-loss spectra and the structural stability of nickel oxide: An LSDA + U study. *Phys. Rev. B* **1998**, *57*, 1505–1509.

[25] Wang, Q. B.; Zhou, C.; Wu, J.; Lü, T. A GGA + U study of the optical properties of vanadium doped ZnO with and without single intrinsic vacancy. *Opt. Commun.* **2013**, *297*, 79–84.

[26] Lin, H.; Wen, Y. W.; Zhang, C. X.; Zhang, L. L.; Huang, Y. H.; Shan, B.; Chen, R. A GGA+U study of lithium diffusion in vanadium doped $LiFePO_4$. *Solid State Commun.* **2012**, *152*, 999–1003.

[27] Wang, L.; Maxisch, T.; Ceder, G. Oxidation energies of transition metal oxides within the GGA + U framework. *Phys. Rev. B* **2006**, *73*, 195107.

[28] Du, A. J.; Sanvito, S.; Smith, S. C. First-principles prediction of metal-free magnetism and intrinsic half-metallicity in graphitic carbon nitride. *Phys. Rev. Lett.* **2012**, *108*, 197207.

[29] Du, A. J.; Sanvito, S.; Li, Z.; Wang, D. W.; Jiao, Y.; Liao, T.; Sun, Q.; Ng, Y. H.; Zhu, Z. H.; Amal, R. et al. Hybrid graphene and graphitic carbon nitride nanocomposite: Gap opening, electron–hole puddle, interfacial charge transfer, and enhanced visible light response. *J. Am. Chem. Soc.* **2012**, *134*, 4393–4397.

[30] Togo, A.; Oba, F.; Tanaka, I. First-principles calculations of the ferroelastic transition between rutile-type and $CaCl_2$-type SiO_2 at high pressures. *Phys. Rev. B* **2008**, *78*, 134106.

[31] Zhang, H.; Liu, L. M.; Lau, W. M. Dimension-dependent phase transition and magnetic properties of VS_2. *J. Mater. Chem. A* **2013**, *1*, 10821–10828.

[32] Ataca, C.; Şahin, H.; Ciraci, S. Stable, single-layer MX_2 transition-metal oxides and dichalcogenides in a honeycomb-like structure. *J. Phys. Chem. C* **2012**, *116*, 8983–8999.

[33] Cheiwchanchamnangij, T.; Lambrecht, W. R. L. Quasiparticle band structure calculation of monolayer, bilayer, and bulk MoS_2. *Phys. Rev. B* **2012**, *85*, 205302.

[34] Zhang, J.; Soon, J. M.; Loh, K. P.; Yin, J. H.; Ding, J.; Sullivian, M. B.; Wu, P. Magnetic molybdenum disulfide nanosheet films. *Nano Lett.* **2007**, *7*, 2370–2376.

[35] Huisman, R.; de Jonge, R.; Haas, C.; Jellinek, F. Trigonal-prismatic coordination in solid compounds of transition metals. *J. Solid State Chem.* **1971**, *3*, 56–66.

[36] Kan, M.; Adhikari, S.; Sun, Q. Ferromagnetism in MnX_2 (X = S, Se) monolayers. *Phys. Chem. Chem. Phys.* **2014**, *16*, 4990–4994.

[37] Kan, M.; Zhou, J.; Sun, Q.; Kawazoe, Y.; Jena, P. The intrinsic ferromagnetism in a MnO_2 monolayer. *J. Phys. Chem. Lett.* **2013**, *4*, 3382–3386.

[38] Kan, M.; Zhou, J.; Sun, Q.; Wang, Q.; Kawazoe, Y.; Jena, P. Tuning magnetic properties of graphene nanoribbons with topological line defects: From antiferromagnetic to ferromagnetic. *Phys. Rev. B* **2012**, *85*, 155450.

[39] Wippermann, S.; Schmidt, W. G. Entropy explains metal–insulator transition of the Si(111) –In nanowire array. *Phys. Rev. Lett.* **2010**, *105*, 126102.

[40] Malliakas, C. D.; Kanatzidis, M. G. Nb–Nb interactions define the charge density wave structure of 2H-$NbSe_2$. *J. Am. Chem. Soc.* **2013**, *135*, 1719–1722.

[41] Mansart, B.; Cottet, M. J. G.; Penfold, T. J.; Dugdale, S. B.; Tediosi, R.; Chergui, M.; Carbone, F. Evidence for a peierls phase-transition in a three-dimensional multiple charge-density waves solid. *Proc. Natl. Acad. Sci. USA* **2012**, *109*, 5603–5608.